The Aeronautical Journal (2026), 1–15
doi:10.1017/aer.2026.10263

RESEARCH ARTICLE

Pilot perception modelling for carrier landing based on Multi-source fuzzy information fusion

Bingyu Li, Shuting Xu, Xin Zhang and Feng Kang

School of Technology, Beijing Forestry University, Beijing, China
Corresponding author: Shuting Xu; Email: xushuting@bjfu.edu.cn

Received: 26 March 2026 UTC; **Revised:** 5 September 2026 UTC; **Accepted:** 5 September 2026 UTC

Keywords: Bayesian regularised neural network; carrier landing; human-machine shared control; multi-source information fusion; pilot perception modelling

Abstract

Carrier-based aircraft landing requires pilots to rapidly integrate heterogeneous cues from the improved Fresnel lens optical landing system, height deviation relative to the reference glide path and the correction trend of height error under strong disturbances and severe time pressure. Such concurrent information processing may lead to perceptual overload and delayed control response. To address this issue, this paper proposes a multi-source information fusion method for pilot perception modelling during carrier-based aircraft landing. First, optical deviation, height deviation and the correction rate of height deviation are fuzzified to construct a unified perceptual feature space. Then, a Bayesian regularised neural network is developed to establish the nonlinear mapping between these inputs and a defuzzified pilot perception proxy index generated by the fuzzy inference system. The results show that the proposed model achieves higher prediction accuracy than conventional regression models and reveals the dominant contribution of height-related information in the perception process. The proposed method provides an interpretable proxy-state representation for pilot-state-aware modelling and offers a potential perceptual basis for future human–machine shared control in carrier-based aircraft landing.

Nomenclature

Δd	optical deviation
Δs	height deviation relative to the reference glide path
Δl	correction rate of height deviation
h	defuzzified pilot perception proxy index
Δu	pilot control correction input
BRNN	Bayesian regularised neural network
DLC	direct lift control
IFLOLS	Improved Fresnel Lens Optical Landing System

Greek symbols

λ	control authority allocation factor

1.0 Introduction

The precise landing of carrier-based aircraft represents a typical high-risk and high-demand scenario in flight control and human–machine cooperation research [1]. This process involves complex aerodynamic coupling and multi-source information interaction, characterised by strong dynamics, high coupling and significant uncertainty [2]. Under strong disturbances and short decision cycles, pilots must

© The Author(s), 2026. Published by Cambridge University Press on behalf of Royal Aeronautical Society.

https://doi.org/10.1017/aer.2026.10263 Published online by Cambridge University Press

rapidly perform attitude adjustment, glide-path correction and thrust coordination [3]. The accuracy of the perception–decision–control chain directly determines flight safety [4, 5]. Therefore, quantitatively analysing pilots' perceptual characteristics and information fusion mechanisms is essential for improving the modelling accuracy of human–machine cooperative landing systems [6, 7].

Existing studies on carrier landing systems mainly focus on aircraft dynamics modelling, control law design and automation strategies, while the modelling of pilot perception and cognitive behaviour has received comparatively limited attention [8, 9]. Some studies employ linear or rule-based approaches to represent pilot perception; however, these models cannot effectively capture the nonlinear coupling among multi-source information, which limits the fidelity of human–machine–environment closed-loop modelling [10, 11]. With the development of human shared control (HSC) and human-in-the-loop control (HILC), researchers have begun to incorporate pilot perceptual states into control systems to achieve adaptive human–machine collaboration and dynamic control authority allocation [12].

During carrier-based aircraft landing, pilots primarily rely on the Improved Fresnel Lens Optical Landing System (IFLOLS) for spatial positioning and glide-path control [13]. However, sensor-derived visual and flight-state measurements are inherently uncertain and subject to perception ambiguity [14]. Previous studies have shown that complex nonlinear relationships exist among optical deviation, attitude variation and longitudinal velocity changes, which conventional control models cannot accurately represent [15]. In typical approach-and-landing tasks, pilots must simultaneously process heterogeneous information sources: the IFLOLS provides optical 'meatball' deviation, while the head-up display (HUD) presents altitude deviation and the rate of altitude correction [16, 17]. The concurrent presentation of these cues can lead to perceptual overload and information competition, increasing the pilot's cognitive burden and risk of misjudgement [18]. Therefore, an effective multi-source information fusion model is required to provide a unified representation of the pilot's comprehensive perception index [19].

To address these challenges, this study adopts a direct lift–based human–machine cooperative landing framework and proposes a multi-source fuzzy information fusion-based modelling method. Fuzzy logic is employed to manage the uncertainty of optical, altitude and correction-trend features, and a Bayesian regularised neural network (BRNN) is developed to analyse the contribution of each information source to a defuzzified pilot perception proxy index h [20, 21]. It should be noted that h is a model-based perceptual proxy generated by the fuzzy inference system, rather than a directly measured physiological or subjective human-factor variable. The effectiveness and robustness of the proposed method are validated through signal processing and simulation experiments in a carrier-landing simulation environment.

The main contributions of this work are summarised as follows:

(1) A carrier-landing-oriented human–machine cooperative framework with a direct-lift-control background is introduced to contextualise pilot perception modelling under multi-source cues.

(2) A multi-source fuzzy information fusion framework is constructed to represent heterogeneous perceptual cues and enhance the interpretability of pilot perception modelling.

(3) A BRNN is developed to estimate the defuzzified pilot perception proxy index h and to reveal the relative contributions of different information sources.

2.0 System architecture

Due to the high risk and complexity of carrier-based aircraft landing tasks, this paper investigates pilot perception and multi-source information fusion within a direct lift control–human–machine shared control system (DLC-HSCS) framework [22, 23]. The overall system architecture is illustrated in Figure 1. The system consists of four hierarchical layers: perception fusion, guidance display, control allocation and shared control strategy. These layers form a closed-loop human–machine–environment coordination structure, providing a systematic foundation for modelling the perception proxy index h. The system adopts direct lift control (DLC) to coordinate thrust and elevator deflection, enabling rapid and precise glide-slope adjustments under low-speed and high angle-of-attack conditions [24].

https://doi.org/10.1017/aer.2026.10263 Published online by Cambridge University Press

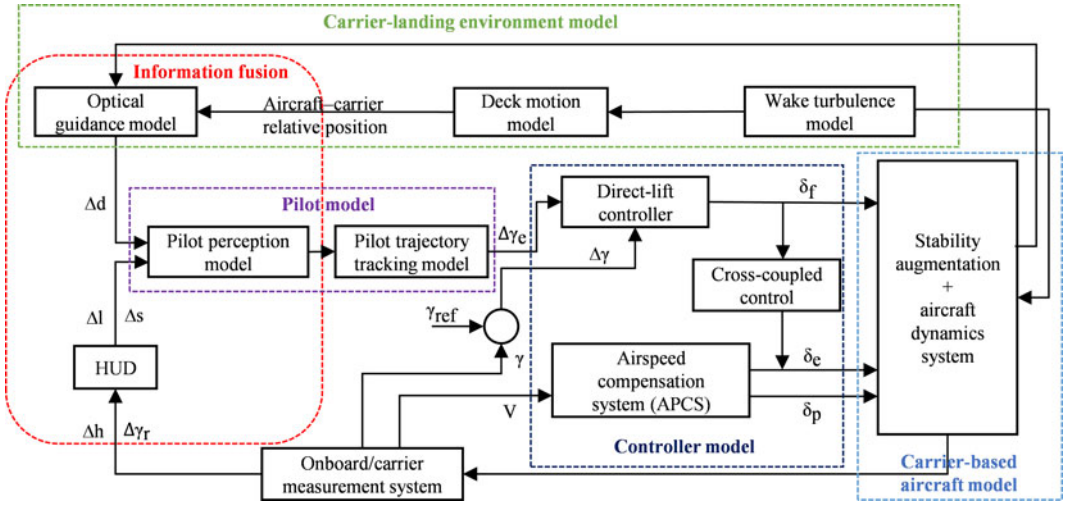


Figure 1. *System modelling and signal-flow architecture, in which the IFLOLS optical deviation* Δd *and the HUD signals* Δs *and* Δl *are integrated to obtain the perception proxy index h.*

As shown in Figure 1, the system modelling and signal-flow framework consists of an environment model, guidance system, pilot model and flight control system. The perception-fusion module integrates three guidance signals: the IFLOLS optical deviation Δd, the HUD height deviation Δs and the HUD height-correction rate Δl. The fuzzy inference system provides a unified reference proxy index h, while the BRNN learns the nonlinear mapping from these three signals to the corresponding perception proxy index. Therefore, the fused signals and the resulting output are explicitly represented as $(\Delta d, \Delta s, \Delta l) \rightarrow h$.

During the landing process, the system continuously acquires the following key state variables:

- Δd: optical deviation of the 'meatball' relative to the IFLOLS reference line, reflecting the glide-slope displacement;
- Δs: height deviation of the aircraft relative to the reference glide path;
- Δl: correction rate of height deviation.

Figure 2 illustrates the physical meanings and geometric relationships of the IFLOLS and HUD guidance signals. The IFLOLS signal Δd represents the meatball displacement relative to the datum-light reference line. In the HUD, Δs represents the vertical deviation between the current aircraft position and the glide-slope reference line (GSRL), whereas Δl reflects the correction trend of the height deviation through the relative position of the velocity-vector guidance symbol. Geometrically, Δd and Δs both reflect the aircraft's departure from the reference glide path from external optical and aircraft-state perspectives, respectively, while Δl indicates the change in this departure associated with the difference between the current and reference trajectory directions. Therefore, Δs describes the current glide-path deviation, while Δl indicates whether this deviation tends to increase or decrease. Together with the external optical cue Δd, these signals provide complementary information on the current deviation and its evolution, forming the physical basis for the subsequent information fusion.

3.0 Multi-source perception fusion method

To achieve quantitative and structured representation of multi-source inputs, a fuzzification framework based on fuzzy logic theory is constructed to process heterogeneous flight information.

https://doi.org/10.1017/aer.2026.10263 Published online by Cambridge University Press

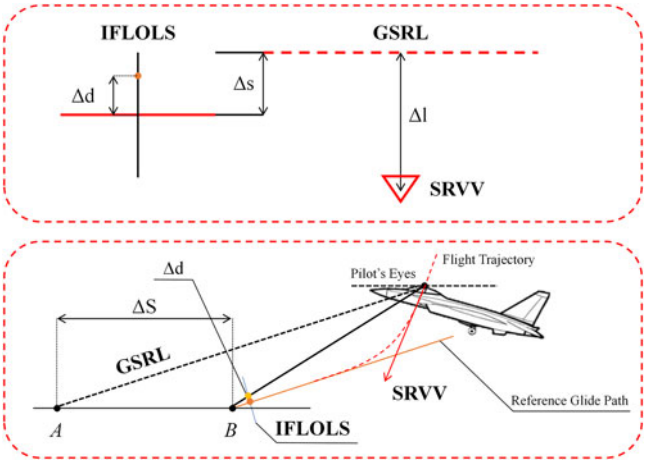


Figure 2. *Physical meanings and relationships of the IFLOLS and HUD guidance signals.*

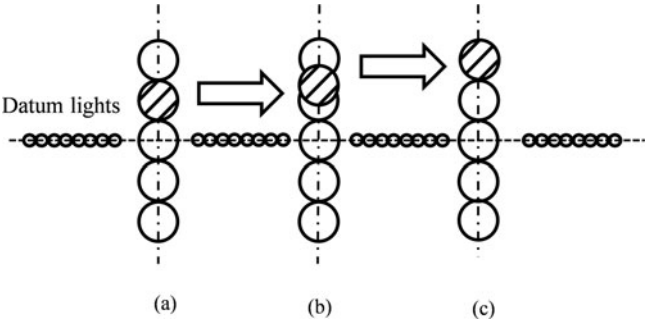


Figure 3. *Fuzzy perception process of optical deviation in the FLOLS: (a) one-ball high; (b) between one-ball and two-balls high; and (c) two-balls high.*

3.1 Optical deviation fuzzification

During carrier-based aircraft landing, pilots determine the height deviation relative to the reference glide path by observing the relative position between the 'meatball' and the datum lights in the Fresnel Lens Optical Landing System (FLOLS). This visual perception process relies heavily on subjective judgement and pilot experience, which introduces inherent uncertainty and ambiguity. Therefore, fuzzy sets are employed to model the optical deviation information, mapping continuously varying optical positions into computational fuzzy states.

As the aircraft deviates from the glide slope, the meatball position varies continuously (Figure 3). Its relative position with respect to the datum lights produces several typical visual states, such as 'one ball high', 'between one and two balls high' and 'two balls high'. These states represent the pilot's fuzzy perception intervals of altitude deviation.

For a five-cell FLOLS system, the input space can be discretised into five representative optical states: (i) the meatball located at the second reference light above the datum light; (ii) the first reference light above the datum light; (iii) aligned with the datum light; (iv) the first reference light below the datum light; and (v) the second reference light below the datum light.

Correspondingly, the output space is quantised into five levels of height deviation: (i) two-balls high deviation; (ii) one-ball high deviation; (iii) on-glide (zero deviation); (iv) one-ball low deviation; and (v) two-balls low deviation.

This input–output relationship forms the basis of the fuzzy inference system.

https://doi.org/10.1017/aer.2026.10263 Published online by Cambridge University Press

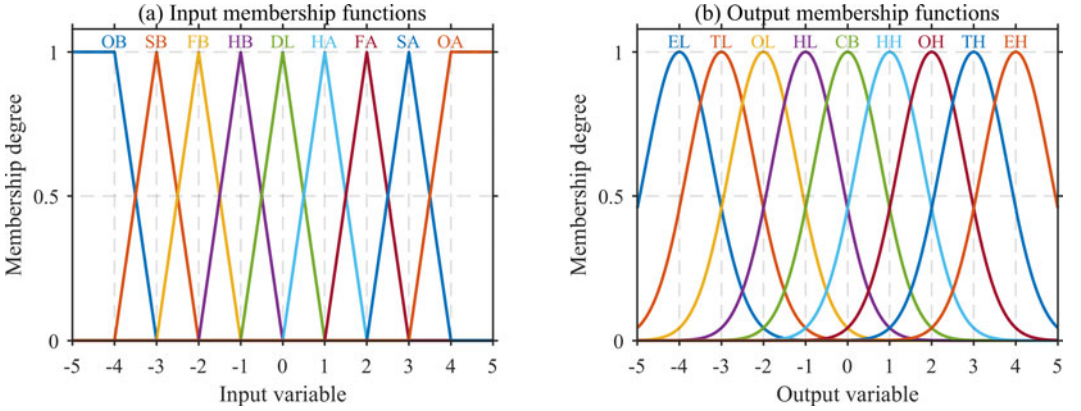


Figure 4. *Membership functions used in pilot perception modelling: (a) input membership functions; (b) output membership functions.*

3.2 Fuzzy perception modelling

To represent the continuous variation of optical deviation, the input variable is modelled using triangular membership functions, consistent with the approximately linear relationship between the optical cue and altitude deviation. The corresponding linguistic variable set is defined as

$$\mathcal{O} = \{\text{OB}, \text{SB}, \text{FB}, \text{HB}, \text{DL}, \text{HA}, \text{FA}, \text{SA}, \text{OA}\} \tag{1}$$

Here, $\mathcal{O}$ denotes the linguistic variable set of the IFLOLS optical position, where OB, SB, FB, HB, DL, HA, FA, SA and OA denote outer below, second below, first below, halfway below, datum line, halfway above, first above, second above, and outer above, respectively.

Considering the subjective uncertainty in pilot perception, the output variable is modelled using Gaussian membership functions to represent the continuously varying perceptual state. The linguistic variable set is defined as

$$\mathcal{P} = \{\text{EL}, \text{TL}, \text{OL}, \text{HL}, \text{CB}, \text{HH}, \text{OH}, \text{TH}, \text{EH}\} \tag{2}$$

Here, $\mathcal{P}$ denotes the linguistic variable set of the perceived height-deviation state, where EL, TL, OL, HL, CB, HH, OH, TH, and EH denote extremely low, two-balls low, one-ball low, half-ball low, centre ball, half-ball high, one-ball high, two-balls high and extremely high, respectively.

The membership functions of the input and output variables are illustrated in Figure 4. The triangular membership functions on the input side reflect the linear geometric distribution of optical cues, whereas the Gaussian membership functions on the output side describe the nonlinear decay of perceptual sensitivity as the deviation increases.

Based on these membership functions, fuzzy input–output mapping rules are constructed to describe the relationship between the input variables and the trajectory stability state. The fuzzy output variable is defined as the trajectory stability state

$$S_h \in [-1, 1] \tag{3}$$

where S_h denotes the fuzzy trajectory stability index, and its linguistic variable set is defined as $\{TH, SH, SS, SL, TL\}$, corresponding to too high, slightly high, stable, slightly low and too low, respectively. The fuzzy inference process adopts the min–max composition operator, and defuzzification is performed using the centroid method. The defuzzified quantitative output is denoted by h, which serves as the reference label for subsequent data-driven modelling and evaluation. It should be noted that h is a model-based cognitive proxy rather than a directly observed physiological variable. In this study, h is introduced to provide a unified and quantitatively tractable representation of the pilot's integrated

https://doi.org/10.1017/aer.2026.10263 Published online by Cambridge University Press

Table 1. *Representative partial fuzzy inference rules under a fixed Δd condition; only representative rules are shown for brevity*

Rule	Δs	Δl	S_h
R1	PU	SD	TH
R2	SU	LD	SH
R3	LL	ST	SS
R4	SD	LA	SL
R5	PD	SA	TL

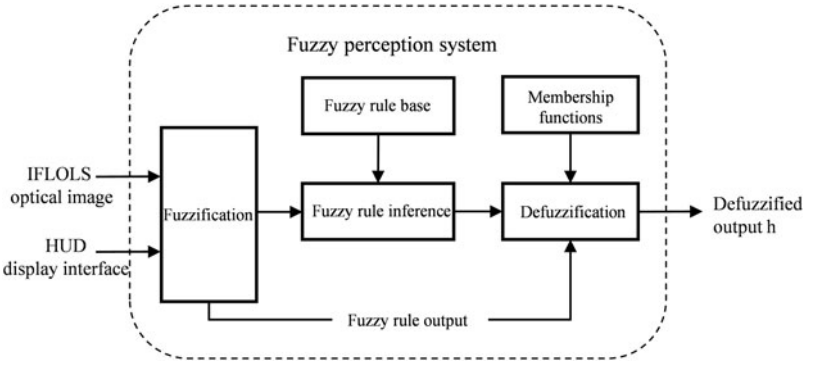


Figure 5. *Architecture of the fuzzy perception system.*

perception of glide-path deviation under multi-source cues. The resulting fuzzy rule base is listed in Table 1. For brevity, Table 1 presents representative rules under a fixed optical-deviation condition, while the complete fuzzy rule base is constructed using the three inputs Δd, Δs and Δl. Here, the linguistic labels of Δs and Δl denote representative fuzzy subsets of height deviation and the correction rate of height deviation, respectively; only representative rules under a fixed Δd condition are listed for brevity.

To achieve a unified semantic representation of multi-source information, the optical deviation, height deviation relative to the reference glide path and the correction rate of height deviation are fuzzified to construct the pilot perception input space. As illustrated in Figure 5, the fuzzy perception system consists of three main modules: fuzzification, fuzzy rule inference and defuzzification. The IFLOLS and HUD information are first processed through fuzzification and then fed into the rule inference module. Fuzzy reasoning is performed based on the fuzzy rule base and membership functions, yielding the fuzzy output state S_h. The defuzzified pilot perception proxy index h is then obtained through centroid defuzzification.

The inference rule can be expressed as

$$\begin{aligned} R_i: \quad & \text{IF } \Delta d \text{ is } A_i,\ \Delta s \text{ is } B_i,\ \text{and } \Delta l \text{ is } C_i, \\ & \text{THEN } S_h \text{ is } D_i \end{aligned} \tag{4}$$

where A_i, B_i and C_i denote the fuzzy subsets of the input variables, and D_i represents the fuzzy subset of the fuzzy output state S_h.

The centroid method is used for defuzzification to obtain the quantitative estimate of the perception proxy index h, which provides structured inputs for the subsequent perception fusion modelling based on a BRNN.

https://doi.org/10.1017/aer.2026.10263 Published online by Cambridge University Press

3.3 BRNN-based perception fusion model

Although fuzzy inference provides a structured representation of multi-source perceptual information, the relationship between the input variables and the perception proxy index h remains highly nonlinear. To capture this nonlinear mapping, a BRNN is adopted for perception fusion modelling.

Compared with conventional neural networks, BRNN introduces Bayesian regularisation into the training process. By incorporating prior distributions of network weights into the loss function, the model automatically balances the trade-off between data fitting and network complexity. This mechanism effectively prevents overfitting and improves generalisation performance, particularly when dealing with noisy or limited data.

The optimisation objective of the BRNN can be expressed as

$$F = \beta E_D + \alpha E_W \tag{5}$$

where E_D denotes the data error term and E_W represents the weight penalty term. The hyperparameters α and β correspond to the precision parameters associated with the weight prior and the data error, respectively. During training, these hyperparameters are automatically updated according to the posterior probability distribution, which balances model complexity and data fitting capability:

$$\alpha = \frac{\gamma}{2E_W}, \qquad \beta = \frac{N - \gamma}{2E_D} \tag{6}$$

where N denotes the total number of samples and γ represents the effective number of network parameters.

The BRNN architecture consists of three input neurons, two hidden layers with 32 and 16 neurons respectively, and one output neuron. The hidden layers employ the *tansig* activation function, while the output layer adopts a *purelin* activation function. The network is trained using the Levenberg–Marquardt (LM) algorithm.

4.0 Results

To quantitatively evaluate the proposed perception fusion model, experimental analyses are conducted based on the fuzzy-processed multi-source perceptual features. Both linear and nonlinear models are constructed to capture the relationships among optical deviation (Δd), height deviation (Δs) and the correction rate of height deviation (Δl). The analysis focuses on prediction accuracy, model robustness and feature contribution, thereby revealing the nonlinear coupling characteristics of the perception proxy index h.

4.1 Data description and preliminary analysis

The experimental data were obtained from a self-developed carrier-based aircraft–carrier landing environment simulation system. The dataset was generated using a self-developed carrier-based landing simulation environment based on an F/A-18 model. In addition, an IFLOLS is embedded to reproduce the visual guidance signals during landing.

The simulation generates multi-source data including flight attitude, velocity, optical deviation and control commands, resulting in a total of 110,137 samples. After synchronisation and normalisation, Δd, Δs and Δl were selected as the input features, while the defuzzified pilot perception proxy index h, generated by the fuzzy inference system, was taken as the output variable. Here, h serves as a model-based reference label for data-driven modelling, rather than a directly observed physiological or subjective pilot-state measurement. The statistical characteristics of the main variables are summarised in Table 2.

To analyse the relationship between the input features and the perception proxy index h, a Pearson correlation analysis was conducted, as shown in Figure 6(a). The results indicate that the height deviation Δs shows the strongest positive linear correlation with h, while the optical deviation Δd also

https://doi.org/10.1017/aer.2026.10263 Published online by Cambridge University Press

Table 2. *Statistical characteristics of key variables during the carrier-landing process*

Variable	Mean	Std	Min	Max
Δd	−0.13308	14.248	−225	268.5
Δs	−0.33421	34.153	−553.8	609.04
Δl	−0.1787	10.144	−96.448	72.383
h	−0.00060477	0.195	−0.92961	0.90575

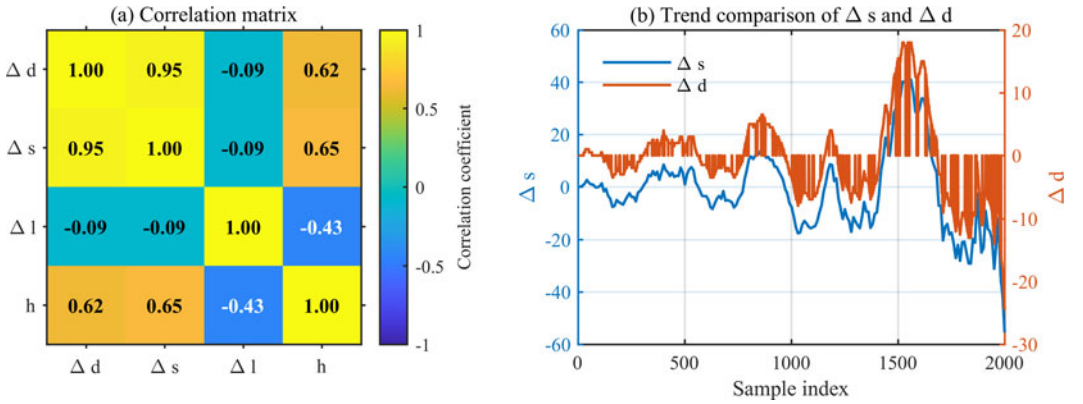


Figure 6. *Correlation of inputs and Δs–Δl dynamic trends: (a) correlation matrix of input features and output; (b) time-series comparison of Δs and Δl.*

exhibits a moderate positive correlation. In contrast, the correction rate of height deviation Δl is negatively correlated with h, suggesting that the correction trend affects the perception index with an opposite sign. These findings imply that Δs and Δd provide more direct linear information about pilot perception, whereas the effect of Δl is sign-dependent and should be further interpreted through nonlinear interaction analysis.

Figure 6(b) presents a typical time-series comparison between Δs and Δl, showing a clear synchronous variation trend. This suggests that height deviation and its correction trend are dynamically coupled during the landing process, and therefore should be jointly considered in subsequent perception modelling.

4.2 Model performance and feature analysis

To investigate the influence of multi-source features on pilot perception, both a linear regression baseline model and a nonlinear BRNN model are constructed.

A multiple linear regression model is first established as

$$h = a_0 + a_1\Delta d + a_2\Delta s + a_3\Delta l + \varepsilon \tag{7}$$

The regression results show that the overall correlation coefficient of the model is $R = 0.753$ ($R^2 = 0.566$), indicating that the linear model can capture the main trend of the perception proxy index h but still presents noticeable residual errors.

Figure 7(a) shows that most samples lie close to the diagonal line. Figure 7(b) illustrates the residual–fitted value distribution, showing that the residuals are generally centred on zero with increased dispersion at higher fitted values. Figure 7(c) presents the normal probability plot of the residuals, indicating that the residuals approximately follow a normal distribution. Overall, the linear model is able to capture the global trend of the perception proxy index h but fails to adequately describe the nonlinear relationships among multi-source perceptual variables.

https://doi.org/10.1017/aer.2026.10263 Published online by Cambridge University Press

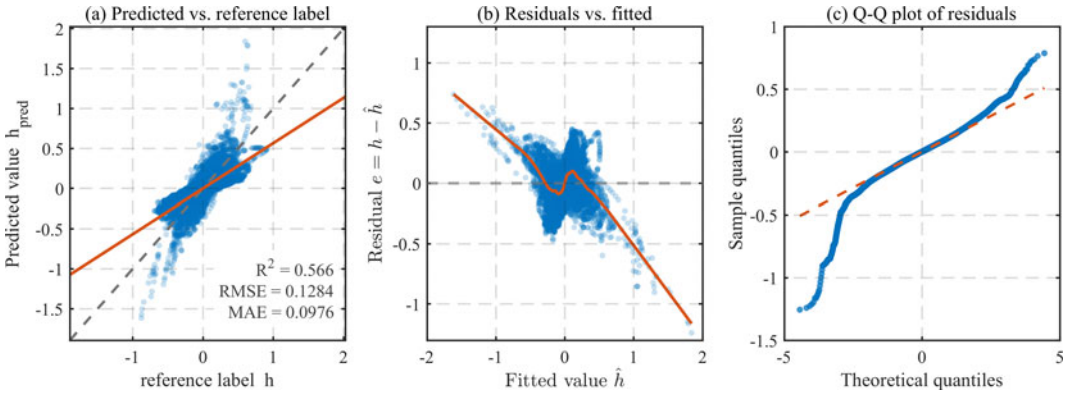


Figure 7. *Linear regression fit and diagnostics: (a) predicted versus reference labels with regression line; (b) residuals versus fitted values; (c) Q-Q plot of residuals.*

The training results are summarised as follows. Training set: $R^2 = 0.8797$, RMSE = 0.0674, MAE = 0.0446. Test set: $R^2 = 0.8780$, RMSE = 0.0691, MAE = 0.0455. Overall performance: $R^2 = 0.882$, MSE = 0.0045.

The prediction performance of the BRNN model is illustrated in Figure 8. Figure 8(a) shows that the predicted values closely follow the reference proxy labels generated by fuzzy inference and are concentrated on the ideal diagonal line. Figure 8(b) further demonstrates that the model accurately captures the dynamic variation of the reference proxy index in the time series.

To evaluate model stability, residual analysis is conducted. The residual is defined as

$$e_i = h_i - \hat{h}_i \tag{8}$$

where h_i denotes the reference proxy label generated by fuzzy inference and $\hat{h}_i$ is the predicted value.

As shown in Figure 8(c)–(d), the residuals approximately follow a zero-mean normal distribution and fluctuate randomly around the zero line, indicating the absence of systematic bias. The cross-validation and feature-combination results are shown in Figure 9. As illustrated in Figure 9(a), the coefficient of determination R^2 obtained from five-fold cross-validation ranges from 0.876 to 0.883, indicating stable prediction performance across different data partitions.

To further analyse the influence of multi-source inputs, feature ablation experiments were conducted using different combinations of Δd, Δs and Δl while keeping the network architecture unchanged. As shown in Figure 9(b), single-feature models provide limited predictive capability. Introducing the posture-related feature Δs significantly improves prediction accuracy ($R^2 = 0.835$), while the fusion of all three features achieves the best performance ($R^2 = 0.879$, RMSE = 0.068, MAE = 0.045). These results indicate that the three perceptual variables exhibit strong complementarity and synergistic effects in modelling the pilot perception index.

Permutation importance analysis shows that the height deviation Δs exhibits the highest contribution (0.845), followed by the correction rate of height deviation Δl (0.153), while the optical offset Δd shows a negligible contribution (0.003). These results indicate that pilot perception is primarily dominated by height deviation, whereas the correction trend plays a secondary role and the direct influence of optical offset is relatively weak. Although Δd shows a moderate pairwise Pearson correlation with h, its marginal contribution becomes negligible after Δs and Δl are jointly considered in the BRNN model, indicating that the information carried by Δd is partly redundant with the other state variables rather than independently dominant. To further reveal the interaction effects between variables, bivariate response surfaces of Δs–Δl and Δd–Δs were constructed, as shown in Figure 10(a) and (b). The results indicate that when Δs is positive, the output h increases correspondingly. Under this condition, a negative deviation in Δl further amplifies the response, suggesting that pilots become more sensitive

https://doi.org/10.1017/aer.2026.10263 Published online by Cambridge University Press

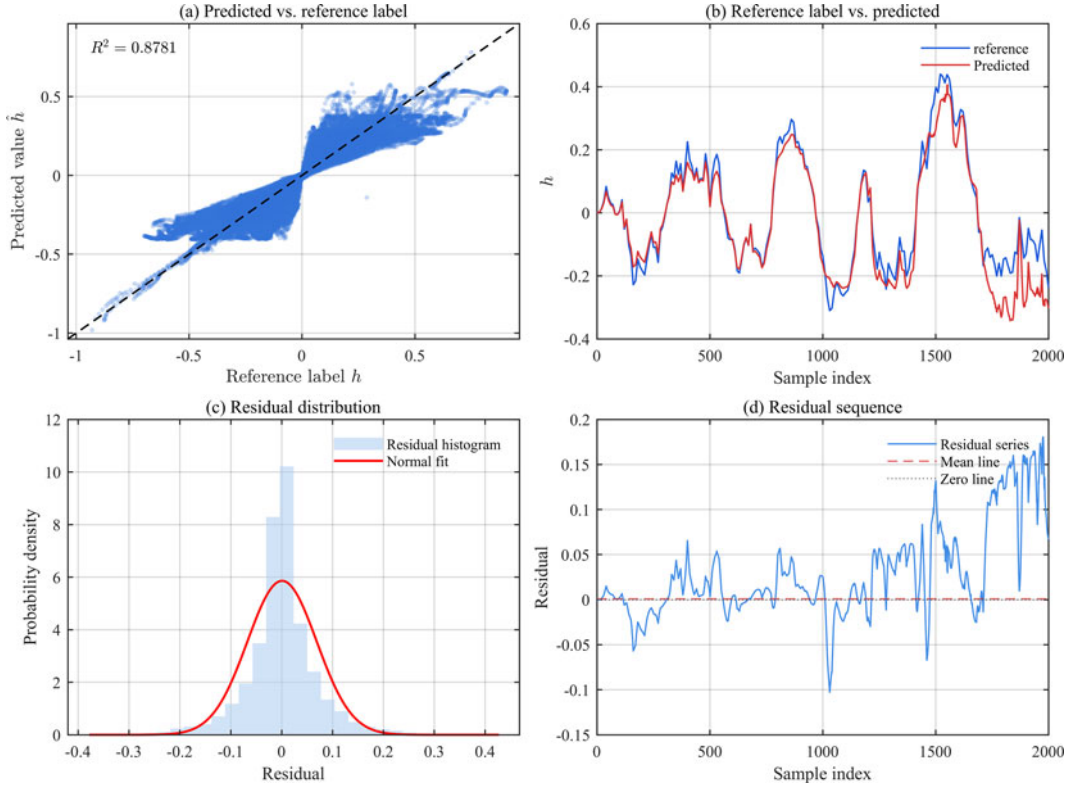


Figure 8. *BRNN prediction performance and residual diagnostics: (a) predicted versus reference labels; (b) comparison of reference and predicted results for the first 2,000 samples; (c) residual distribution with normal fit; (d) residual sequence with mean and zero reference lines.*

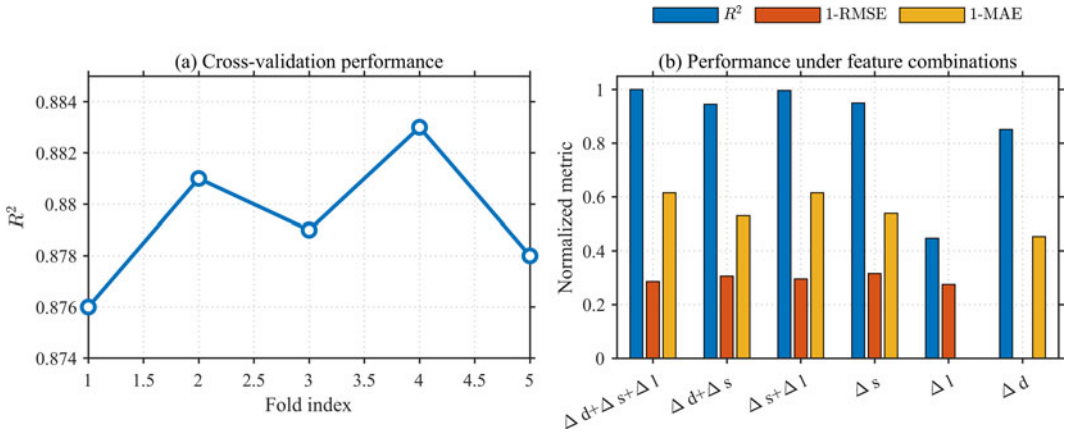


Figure 9. *Model validation and feature-combination evaluation: (a) five-fold cross-validation performance in terms of R^2; (b) performance comparison under different feature combinations based on normalised metrics.*

https://doi.org/10.1017/aer.2026.10263 Published online by Cambridge University Press

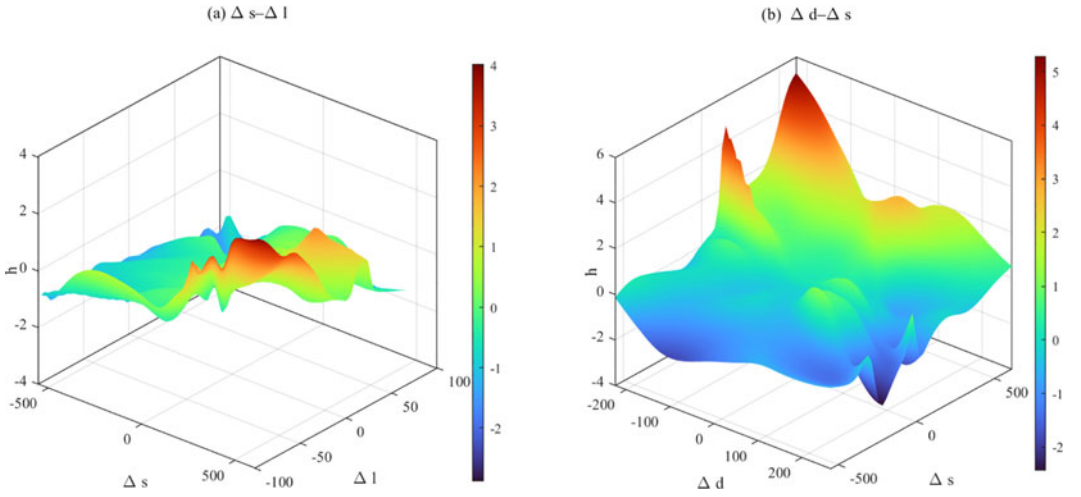


Figure 10. *Feature importance and nonlinear interaction results: (a) Δs–Δl response surface; (b) Δd–Δs response surface.*

to altitude variations during the posture correction phase. Furthermore, the Δd–Δs surface exhibits a tilted band-like distribution. When Δd and Δs vary in the same direction, the predicted pilot perception index $\hat{h}$ increases; otherwise, the response decreases.

Overall, pilot perception during carrier landing follows a multi-source fusion pattern characterised by altitude-deviation dominance, correction-trend assistance and weak independent optical contribution. These contribution patterns may provide a candidate basis for parameterising control-authority regulation in future human–machine shared-control design. As an application-oriented interpretation of the feature-contribution results, a candidate control-authority allocation function can be formulated as

$$\lambda(t) = \frac{1}{1 + \exp[-k(\Delta u - \Delta u_0)]} \tag{9}$$

where k is the sensitivity coefficient, Δu represents the pilot control input deviation and Δu_0 denotes the takeover threshold.

According to the feature-importance weights ($w_s = 0.845$, $w_l = 0.153$ and $w_d = 0.003$), the sensitivity coefficient k is defined as

$$k = k_0\,(0.845|\Delta s| + 0.153|\Delta l| + 0.003|\Delta d|). \tag{10}$$

where k_0 is a normalisation coefficient.

Under this formulation, larger perceived deviation levels would lead to a higher sensitivity of control-authority adjustment. This relationship is intended as a physically interpretable application of the perception model, rather than a fully validated shared-control law in the present study.

5.0 Discussion

To further examine the practical implications of the proposed perception model, simulation-based validation and robustness analysis were conducted in a closed-loop carrier-landing environment. Pilot-model–aircraft closed-loop simulations were performed using the integrated carrier-based aircraft–carrier–IFLOLS simulation framework shown in Figure 1. The framework integrates the carrier environment, IFLOLS and HUD guidance systems, the pilot perception and trajectory-tracking models, the direct-lift controller and the aircraft dynamics.

https://doi.org/10.1017/aer.2026.10263 Published online by Cambridge University Press

Table 3. *Landing performance in 50 fusion-assisted closed-loop simulations*

Performance metric	Result
Signed mean touchdown deviation (m)	0.839
Standard deviation (m)	3.418
Successful landings, n/N (%)	50/50 (100%)
Ideal landings, n/N (%)	47/50 (94%)

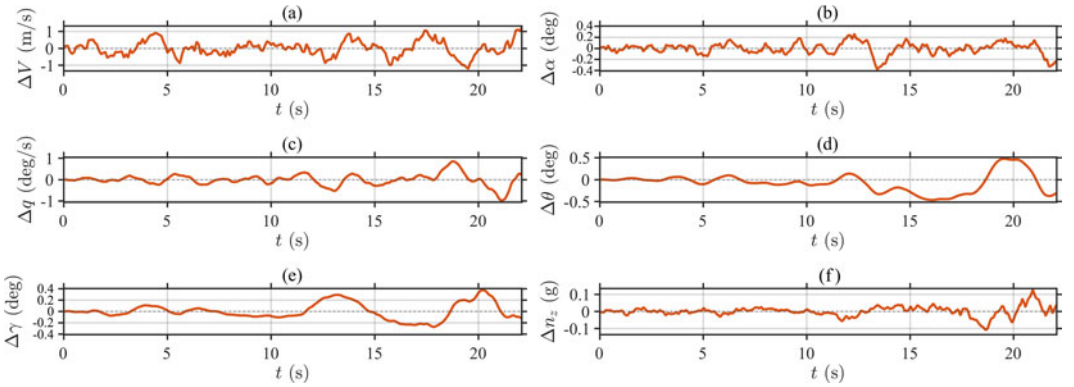


Figure 11. *Aircraft-state variations during a representative fusion-assisted closed-loop landing.*

A total of 50 closed-loop landing simulations were performed using the fused IFLOLS and HUD guidance information under the prescribed deck-motion conditions.

Figure 11 presents the aircraft-state variations during a representative fusion-assisted closed-loop landing. The representative simulation was selected as the run whose altitude-deviation root mean square error (RMSE) was closest to the median value across the 50 simulations. In this configuration, the perception proxy index h derived from Δd, Δs and Δl was supplied to the pilot trajectory-tracking model. The aircraft states remained bounded throughout the selected landing.

Landing performance was evaluated using the touchdown-point deviation. A landing was classified as successful when the touchdown point remained within ± 12.2 m of the reference point, while an ideal landing was defined using the more restrictive range of ± 6.1 m. The signed mean and standard deviation of the touchdown-point deviation were used to characterise touchdown bias and dispersion, respectively.

Table 3 summarises the resulting landing-performance statistics. The fusion-assisted configuration achieved a signed mean touchdown deviation of 0.839 m and a standard deviation of 3.418 m. The observed landing success rate was 100%, while the ideal landing rate was 94% under the investigated simulation conditions.

To further investigate the predictive robustness of the BRNN model, Gaussian noise with intensities of 1%, 2% and 5% of the standard deviation of each input feature was added to the test inputs. For each noise level, 20 independent noise realisations were evaluated using the same trained model and test samples. As shown in Figure 12(a), R^2 decreases from 0.8769 under the noise-free condition to 0.8590 at the 5% noise level, while RMSE and mean absolute error (MAE) increase from 0.0682 and 0.0450 to 0.0730 and 0.0532, respectively. These results indicate that the model retains comparatively stable predictive performance under the investigated input disturbances.

Figure 12(b) shows the relative changes with respect to the noise-free condition. In Figure 12(c), the colour scale represents the performance-retention score relative to the noise-free baseline, with a higher score indicating better performance. The numerical annotations show the original metric values.

https://doi.org/10.1017/aer.2026.10263 Published online by Cambridge University Press

Table 4. *Performance comparison of regression models*

Model	R^2	RMSE	MAE
LR	0.566	0.128	0.098
SVR	0.873	0.069	0.044
GPR	0.826	0.081	0.050
BRNN	0.882	0.068	0.045

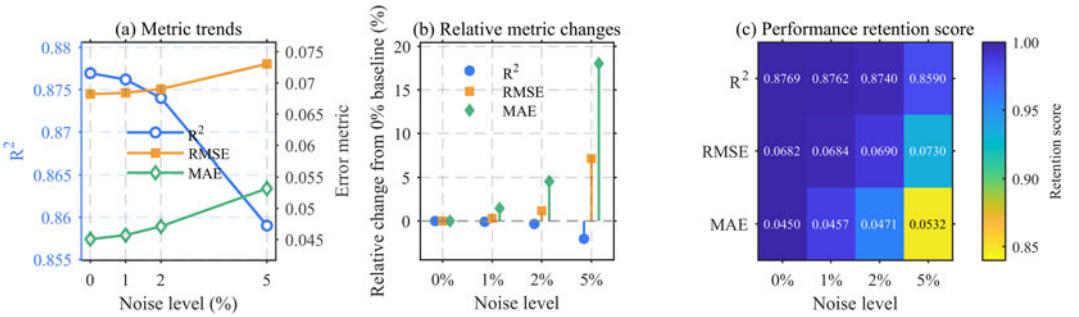


Figure 12. *BRNN robustness under different input-noise levels: (a) metric trends; (b) relative changes; (c) performance-retention scores.*

To further evaluate model performance, four regression models were tested on the same dataset, including linear regression (LR), support vector regression (SVR) with a radial basis function (RBF) kernel, Gaussian process regression (GPR) and BRNN. As shown in Figure 13, BRNN follows the reference labels more closely than the other models. Consistent with this observation, Table 4 shows that BRNN achieves the best overall performance ($R^2 = 0.882$, RMSE = 0.068 and MAE = 0.045), followed by SVR. LR fails to capture the nonlinear relationship, while GPR shows lower accuracy than BRNN and SVR.

The proposed method is currently applicable to the final-approach phase of carrier landing using the three guidance variables considered in this study. Its generalisation to other aircraft, operating conditions and guidance-information combinations requires further investigation. Moreover, the index h is a fuzzy-inference-based proxy rather than a directly measured pilot state, and the present validation is mainly based on simulation data and Gaussian input noise. The closed-loop evaluation is limited to 50 simulations under the present carrier-air disturbance and deck-motion settings. Therefore, future work will include pilot-in-the-loop validation, comparison with subjective or physiological measurements, and evaluation under more diverse disturbances and operating conditions.

6.0 Conclusion

This study addresses the perceptual burden imposed by multi-source information during carrier landing. A BRNN-based fusion method is proposed to estimate the defuzzified pilot perception proxy index h.

First, fuzzy logic is employed to achieve a unified representation of multi-source information, including optical deviation, height deviation and the correction rate of height deviation, thereby providing structured inputs for perception modelling. Subsequently, a BRNN-based fusion model is constructed to predict the perception proxy index h through nonlinear mapping, achieving a prediction accuracy of $R^2 = 0.882$. Feature contribution analysis indicates that the height deviation Δs plays a dominant role, the correction trend Δl acts as auxiliary information, while the optical deviation Δd has a relatively minor independent effect. Finally, simulation-based evaluations demonstrated the predictive robustness of the proposed model. The closed-loop landing simulations further demonstrated the feasibility of

https://doi.org/10.1017/aer.2026.10263 Published online by Cambridge University Press

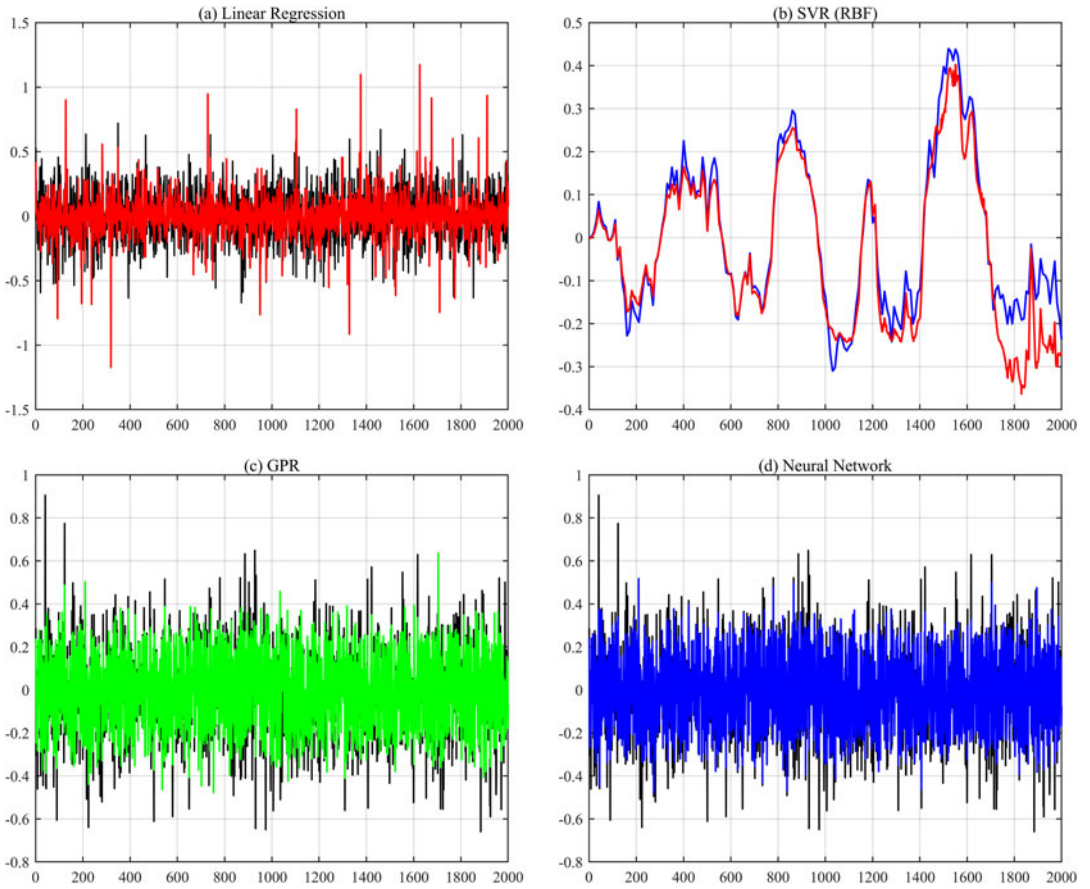


Figure 13. *Comparison of regression models for estimating the perception proxy index h: (a) LR; (b) SVR; (c) GPR; (d) BRNN.*

incorporating the fused guidance information into the pilot trajectory-tracking framework under the investigated simulation conditions.

Acknowledgements. This study was supported by the National Natural Science Foundation of China (Grant No. 12402413).

References

[1] Tokadli, G., Dorneich, M.C. and Matessa, M. Toward human–autonomy teaming in single-pilot operations: domain analysis and requirements, *J. Air Transp.*, 2021, **29**, pp 142–152. https://doi.org/10.2514/1.D0240.

[2] Wu, L., Deng, Y. and Duan, H. Optimization-based automatic carrier landing control with pilot model and approaching power compensation, *Aerosp. Sci. Technol.*, 2025, **164**, p 110387. https://doi.org/10.1016/j.ast.2025.110387.

[3] Duan, H., Chen, L. and Zeng, Z. Automatic landing for carrier-based aircraft under the conditions of deck motion and carrier airwake disturbances, *IEEE Trans. Aero Electr. Syst.*, 2022, **58**, pp 5276–5291. https://doi.org/10.1109/TAES.2022.3168247.

[4] Yu, W., Jin, D., Zhao, F. and Zhang, X. Towards pilot's situation awareness enhancement: a framework of adaptive interaction system and its realization, *ISA Trans.*, 2023, **132**, pp 109–119. https://doi.org/10.1016/j.isatra.2022.12.005.

[5] Luzzani, G., Buraioli, I., Demarchi, D. and Guglieri, G. A review of physiological measures for mental workload assessment in aviation, *The Aeronaut. J.*, 2024, **128**, pp 928–949. https://doi.org/10.1017/aer.2023.101.

[6] Zhu, W., Xie, Y., Wang, Y., Zhang, C., Yuan, J., Chen, H., Zuo, X., Jiang, C. and Wang, T. Classification of carrier-based aircraft pilot mental workloads based on feature-level fusion and decision-level fusion of PPG and EEG signals, *The Aeronaut. J.*, 2025, **129**, pp 2757–2776. https://doi.org/10.1017/aer.2025.33.

[7] Singh, G., Chanel, C.P.C. and Roy, R.N. Mental workload estimation based on physiological features for pilot-UAV teaming applications, *Front. Hum. Neurosci.*, 2021, **15**, p 692878. https://doi.org/10.3389/fnhum.2021.692878.

https://doi.org/10.1017/aer.2026.10263 Published online by Cambridge University Press

[8] Kyle, A.R., Rouser, B., Paul, R.C. and Jurewicz, K.A. Quantifying pilot performance and mental workload in modern aviation systems: a scoping literature review, *Aerospace*, 2025, **12**, p 626. https://doi.org/10.3390/aerospace12070626.
[9] Lyons, J.B., Sycara, K., Lewis, M. and Capiola, A. Human–autonomy teaming: definitions, debates, and directions, *Front. Psychol.*, 2021, **12**, p 589585. https://doi.org/10.3389/fpsyg.2021.589585.
[10] Wang, W., Na, X., Cao, D., Gong, J., Xi, J., Xing, Y. and Wang, F.-Y. Decision-making in driver-automation shared control: a review and perspectives, *IEEE/CAA J. Autom. Sinica*, 2020, **7**, pp 1289–1307. https://doi.org/10.1109/JAS.2020.1003294.
[11] Bernabei, M. and Costantino, F. Adaptive automation: status of research and future challenges, *Robot. Comput.-Integr. Manuf.*, 2024, **88**, p 102724. https://doi.org/10.1016/j.rcim.2024.102724.
[12] Schwerd, S. and Schulte, A. Operator state estimation to enable adaptive assistance in manned–unmanned teaming, *Cognit. Syst. Res.*, 2021, **67**, pp 73–83. https://doi.org/10.1016/j.cogsys.2021.01.002.
[13] Zhang, Z. and Zhen, Z. Research progress on guidance and control of fixed-wing manned and unmanned carrier-based aircraft landing, *Acta Aeronaut. et Astronaut. Sinica*, 2025, **46**, p 532336. https://doi.org/10.7527/S1000-6893.2025.32336.
[14] Luo, S., Zhang, C., Zhu, W., Chen, H., Yuan, J., Li, Q., Wang, T. and Jiang, C. Noncontact perception for assessing pilot mental workload during the approach and landing under various weather conditions, *Signal, Image Video Process.*, 2025, **19**, p 98. https://doi.org/10.1007/s11760-024-03619-x.
[15] Efremov, A.V. and Prodanik, V.A. Identification of the characteristics of pilot control actions in a multichannel control task with cross-coupling, *Aerospace Syst.*, 2025. https://doi.org/10.1007/s42401-025-00391-9.
[16] Blundell, J., Scott, S., Harris, D., Huddlestone, J. and Richards, D. Workload benefits of colour coded head-up flight symbology during high workload flight, *Displays*, 2020, **65**, p 101973. https://doi.org/10.1016/j.displa.2020.101973.
[17] Li, W.-C., Zhang, J., Court, S., Kearney, P. and Braithwaite, G. The influence of augmented reality interaction design on pilot's perceived workload and situation awareness, *Int. J. Ind. Ergonom.*, 2022, **92**, p 103382. https://doi.org/10.1016/j.ergon.2022.103382.
[18] Liu, C., Zhang, C., Zhu, W., Jiao, S., Zhang, Y., Xu, R. and Liang, Y. Measuring pilot mental workload during flights without PAPI lights using a wearable device, *Appl. Psychophys. Biofeedback*, 2026, **51**, pp 235–248. https://doi.org/10.1007/s10484-025-09729-7.
[19] Xu, R., Cao, S., Barnett-Cowan, M., Bulbul, G., Irving, E., Niechwiej-Szwedo, E. and Kearns, S. An in-flight multimodal data collection method for assessing pilot cognitive states and performance in general aviation, *MethodsX*, 2025, **15**, p 103589. https://doi.org/10.1016/j.mex.2025.103589.
[20] Hüllermeier, E. and Waegeman, W. Aleatoric and epistemic uncertainty in machine learning: An introduction to concepts and methods, *Mach. Learn.*, 2021, **110**, pp 457–506. https://doi.org/10.1007/s10994-021-05946-3.
[21] Lampinen, J. and Vehtari, A. Bayesian approach for neural networks—review and case studies, *Neural Netw.*, 2001, **14**, pp 257–274. https://doi.org/10.1016/S0893-6080(00)00098-8.
[22] Wu, Q. and Zhu, Q. Fault-tolerant control of automatic carrier landing using direct lift control based on nonsingular terminal sliding mode and active disturbance rejection control, *Trans. Inst. Measur. Control*, 2025, **47**, pp 29–40. https://doi.org/10.1177/01423312241241104.
[23] Varriale, C., Lombaerts, T. and Looye, G. Direct lift control: a review of its principles, merits, current and future implementations, *Prog. Aerosp. Sci.*, 2025, **152**, p 101073. https://doi.org/10.1016/j.paerosci.2024.101073.
[24] Yao, Z., Kan, Z., Li, D., Shao, H., Jiang, Y. and Xiang, J. Active anti-disturbance carrier landing control with integrated direct lift, *Comput. Electr. Eng.*, 2024, **120**, p 109699. https://doi.org/10.1016/j.compeleceng.2024.109699.

Cite this article: Li B., Xu S., Zhang X. and Kang F. Pilot perception modelling for carrier landing based on Multi-source fuzzy information fusion. *The Aeronautical Journal*, https://doi.org/10.1017/aer.2026.10263

https://doi.org/10.1017/aer.2026.10263 Published online by Cambridge University Press